2007

Microstructure evolution and microstructure - property relationships in friction stir processing of NiAl bronze

McNelley, T.R.; Oh-Ishi, K.; Zhilyaev, A.P.

Trans Tech Publications

T.R. McNelley, K. Oh-Ishi, A.P. Zhilyaev, "Microstructure evolution and Microstructure - property relationships in friction stir processing of NiAl bronze," Material Science Forum, v.539-543, (2007) pp. 3745-3750.
https://hdl.handle.net/10945/55344

Materials Science Forum *Online: 2007-03-15*
ISSN: 1662-9752, Vols. 539-543, pp 3745-3750
doi:10.4028/www.scientific.net/MSF.539-543.3745

MICROSTRUCTURE EVOLUTION AND MICROSTRUCTURE – PROPERTY RELATIONSHIPS IN FRICTION STIR PROCESSING OF NiAl BRONZE

T.R. McNelley[1,a], K. Oh-ishi[1,2,b] and A.P. Zhilyaev[1,3,c]

[1] Department of Mechanical and Astronautical Engineering, Naval Postgraduate School, 700 Dyer Road, Monterey, CA 93943-5146, USA

[2] Present address: National Institute for Materials Science, 1-2-1 Sengen, Tsukuba 305-0047 Japan

[3] On leave from Institute for Metals Superplasticity Problems, Russian Academy of Science, 39 Khalturinia, Ufa, 450001 Russia

[a] tmcnelley@nps.edu, [b] masakei1@yahoo.co.jp, [c]AlexZ@anrb.ru

Keywords: Friction stir processing; NiAl Bronze; As-cast; Porosity; Grain refinement; Ductility.

Abstract. Friction stir processing (FSP) has been employed for localized modification and control of microstructures in NiAl bronze materials, which are widely utilized for marine components. The thermomechanical cycle of FSP results in homogenization and refinement and the conversion of microstructures from a cast to a wrought condition within stir zones in the material. However, the direct measurement of stir zone temperatures, strains, strain rates and cooling rates is difficult due to steep gradients and transients in these quantities, and this is an impediment in the assessment of FSP-induced microstructures and properties. Quantitative microstructure analyses following FSP of cast NiAl bronze materials have been used to develop estimates of stir zone thermomechanical cycles. The estimation procedures will be reviewed and the microstructure-based estimates will be compared to results from computational models and embedded thermocouples measurements. Stir zone microstructures comprise a mixture of primary α grains and transformation products of the β that formed during processing. Recrystallization in the primary α occurred due to particle-stimulated nucleation in this low stacking fault energy material. Factors that influence the distribution of strength and ductility in the stir zone appear to include the mixture of microstructure constituents and gradients in microstructure due to gradients in processing conditions.

Introduction

FSP is an adaptation of friction stir welding (FSW), a solid-state joining process originally developed at The Welding Institute [1]. FSP enables localized modification and control of microstructures in near-surface layers of metallic components [2, 3, 4]. In the process, a cylindrical, wear-resistant tool consisting of a smaller diameter pin with a concentric, larger-diameter shoulder is rotated and forced into the surface of the work piece. As the tool penetrates, a combination of frictional and adiabatic heating softens the material so that tool rotation induces a stirring action and flow of material about the pin. The severe, but localized, plastic deformation results in formation of a stir zone (SZ) while adjacent regions that experience only moderate straining comprise the thermomechanically affected zone (TMAZ). Large areas may be processed by traversing the tool in a pattern on the work piece surface. FSP has been employed to homogenize and refine microstructures in both cast and wrought metals, including alloys of Al [5, 6, 7, 8, 9, 10] and Mg [11, 12] and higher melting alloys of Cu [13], Fe [14] and Ti [15]. Benefits of FSP in cast metals include elimination of porosity and local conversion of cast microstructures to a wrought condition, with enhanced surface properties. Significantly improved strength/ductility combinations [16, 17] and high-strain-rate superplasticity [5, 6, 7, 8, 9, 18] have been achieved by FSP of wrought materials.

The FSP/W thermomechanical cycle likely induces recrystallization and phase transformations but direct measurement of SZ temperatures, strains and strain rates is difficult due to steep gradients and transients in these quantities, and this impedes the assessment of processing-induced microstructures.

Table 1. FSP parameters for samples examined in this investigation

Process Designator	Rotation Rate (rpm)	Traversing Rate (mm m^{-1})	Tool Advance per Revolution (mm/rev)
FSP516	800	152	0.191
FSP520	1000	203	0.203

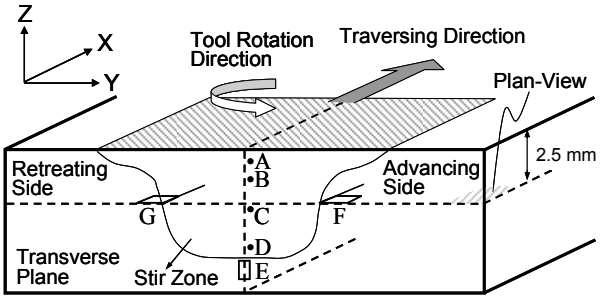

Fig.1. A schematic of the SZ illustrates the locations (A – G) from which data were acquired. The coordinate axes correspond to the standard axes for FSP

For this reason, quantitative microstructure analysis following FSP of cast NAB materials has been used to develop estimates of local peak SZ temperatures and details of the estimation procedure have been given in previous reports [19, 20]. Briefly, during cooling at rates ~10^{-3} ºCs^{-1} after casting, the NAB solidifies as a single-phase β bcc solid solution. The primary α constituent forms from the β with a Widmanstätten morphology during subsequent cooling;. Globular precipitates which are Fe_3Al having a DO_3 structure and designated κ_{ii} also form from the β and attain sizes of 20 – 30 μm, and, at lower temperatures, finer Fe_3Al precipitates designated κ_{iv} form in the primary α and are 1 - 10 μm in size. A eutectoid reaction, $\beta \rightarrow \alpha + \kappa_{iii}$, takes place at ~800 ºC. The κ_{iii} is nominally NiAl having a B2 structure. Thus, following such equilibrium cooling the microstructure of this as-cast NAB consists of a primary α fcc terminal solid solution, which contains a fine dispersion of κ_{iv} precipitate particles, and a eutectoid constituent, $\alpha + \kappa_{iii}$, which contains coarse, globular κ_{ii} particles.

After FSP, SZ microstructures in NAB materials generally include primary α, non-equilibrium transformation products of the β phase, κ_{ii}, and, in some locations, κ_{iv}. These microstructures depend strongly on local peak temperatures and subsequent cooling rates. Altogether, the absence of the $\alpha + \kappa_{iii}$ eutectoid constituent as well as the presence of non-equilibrium β transformation products, including fine Widmanstätten α, bainite and martensite, indicate local heating to temperatures above the eutectoid (~800 °C). The relative fractions of the primary α, the β transformation products and the κ_{ii} and κ_{iv} have been employed to estimate local peak temperatures in conjunction with data on phase equilibria in NAB alloys. These estimates assume local equilibrium due to acceleration of diffusion-controlled reactions by excess vacancy generation during deformation and heating to the local peak temperature [21, 22, 23]. The morphologies of the primary α and the β transformation products depend on the details of the local thermomechanical history, but also suggest that the α and β phases experience compatible deformation during straining at $T \geq 800$°C. A detail discussion of the β transformation products that form during cooling after passage of the tool has already been provided [19, 20]. The effects of deformation and recrystallization processes within the primary α are retained after FSP and these processes are the subject here. Microstructure and microtexture data were acquired in the fcc α phase of the SZ and surrounding TMAZ by use of OIM and TEM methods in order to evaluate the deformation and recrystallization processes that resulted from the FSP.

Experimental Procedures

The material examined in this investigation is UNS C95800 NAB, and details of the specification and composition have been included in previous reports [19, 20]. FSP was accomplished at the Rockwell Scientific Company, Thousand Oaks, CA with tools machined from MP159, an alloy having a

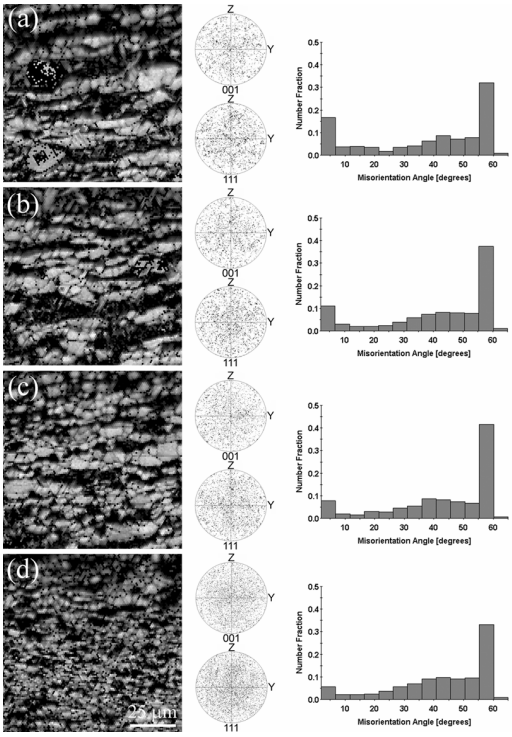

Fig. 2. OIM data from the SZ illustrating random orientations in the primary α and random grain to grain misorientation distributions with distrnutions of twin and low angle boundaries superimposed.

nominal composition of 25Ni – 36Co – 19Cr – 9Fe – 7Mo – 3Ti (wt pct). Details of the tool design have also been given previously [19, 20]; briefly, the tools had a shoulder diameter of 23.8 mm, a pin diameter of 7.95 mm and a pin depth of 6.65 mm; additionally, the pin had a spiral groove. Two processing conditions from prior work were selected for the present study. These were: 1) tool rotation and traversing rates of 800 rpm and 152 mm m^{-1} (6 in m^{-1}), respectively; and 2), rotation and traversing rates of 1000 rpm and 203 mm m^{-1} (8 in m^{-1}). In both cases, the tool axis was inclined ~ 3º opposite to the direction of tool advance and the process involved a single traverse approximately 200 mm in length under X-axis displacement rate control. The ratio of the traversing rate to the rotation rate, i.e., tool advance per revolution (Table 1; the designators are only serial numbers), is essentially the same for these two samples; accordingly the SZ microstructures are similar and have been discussed in previous reports [19, 20]. The conventional axes for FSP are included in the schematic of Fig. 1; the tool traverses in the X direction, Y is the longitudinal direction, and Z is the plate normal direction. In Fig. 1, the Y – Z plane is the transverse plane; here, a plan view of the SZ was obtained in a plane 2.5 mm below the plate surface and parallel to the X – Y plane. Locations of various analyses are indicated in Fig. 1. Microtexture analysis by orientation image microscopy (OIM) was conducted using a Topcon SM-510 scanning electron microscope (SEM) equipped with a tungsten filament and operated at 20 kV. OIM was conduced at the locations indicated in Fig. 1. Sample preparation has been described previously [19, 20]. Standard methods of data acquisition and analysis were employed to evaluate microstructure and texture in the primary α grains. Transmission electron microscopy (TEM) was accomplished with a Topcon 002B microscope equipped with a LaB_6 filament and operated at 200 kV. Samples for TEM examination were obtained by standard methods. Convergent-beam electron diffraction (CBED) patterns were taken from each α phase grain in a region of contiguous grains and the patterns were then analyzed to determine unambiguous lattice orientations of the grains. The orientation of the CBED pattern captured from each grain was indexed with an accuracy of ~0.2º using the Tools for Orientation Crystallographic Analysis (TOCA) software (EDAX-TSL, Inc.) for TEM. The grain-to-grain lattice disorientation accuracy was then ~0.4º. Optical microscopy (OM) involved standard sectioning and preparation methods; etched samples were examined using bright-field (BF) illumination in a Zeiss Jenaphot 2000 equipped with a digital imaging system.

Results and Discussion

Inside the SZ. Fig. 2 shows representative OIM data from the SZ in FSP516. These data are in the form of image-quality (IQ) maps, discrete (001) and (111) pole figures, and histograms representing the grain-to-grain misorientation angle distributions in the α phase. Detailed OM and TEM analysis of the β transformation products at these SZ locations for the processing conditions of Table I have been previously reported by the authors [19]. Here, higher IQ in the EBSD patterns corresponds to brighter gray tones in the maps; the corresponding areas in the maps are mainly the primary α that persisted during processing. Locations of low IQ during scanning may reflect locations near α-phase grain

boundaries, undissolved κ_{ii}, or fine, complex β transformation products. The banded distribution of primary α and β transformation products in Fig. 2 agrees with previous OM analysis of this material [19]. The primary α grain size becomes finer with depth in the SZ and is finest at the bottom, i.e. the location of Fig. 2(d) which is location D in Fig. 1. Throughout the SZ the discrete pole figure data shows only random orientations in the α phase. In contrast, distinct shear textures in the SZ in FSP/W of aluminum alloys [14, 15 ,24] have been reported. The observation here of random textures within the SZ is indicative of recrystallization involving the formation of randomly oriented grain nuclei followed by migration of high angle boundaries during the thermomechanical cycle of FSP. The distributions of grain-to-grain misorientation angles for all locations show a distinct random component, which is similar to that predicted by MacKenzie for randomly oriented cubes [25], but with additional peaks at 0 - 5° and at 60°. The low-angle boundaries may reflect deformation of newly recrystallized grains by the tool shoulder after passage of tool pin. At all SZ locations there is a distinct population of ~ 60º boundaries that likely reflects the formation of annealing twins after recrystallization during FSP. The results of TEM/TOCA analysis for location D near the boundary of the SZ under the tool pin are shown in Fig. 3. Fig. 3(a) is a TEM image suggesting that highly refined α grains 1 - 2 μm in size are attained in this location by the processing. The boundaries in this image are shown in the tracing of the boundaries in Fig. 3(b) in which the line width corresponds to the grain-to-grain disorientation angles from TOCA analysis. The hatched areas indicate locations comprising either κ_{ii} or κ_{iv} constituent particles that were deformed or broken up by processing. Most of the boundaries are of high disorientation angle, $\theta > 40º$; these are indicated by thickest lines, and many of these are twin boundaries of approximately 60º disorientation.

Locations along the SZ/TMAZ interface. Fig. 4(a) shows a montage of optical micrographs from the plan-view plane on the advancing side of the SZ for FSP520. This plane is at about half of the SZ depth and corresponds to location F as shown in Fig. 1. The tool traversing direction is upward. Figs. 4(b) - (d) show OIM results obtained from the region delineated by the dotted frame in Fig. 8(a); this region spans the distinct interface between the TMAZ and SZ, and the TMAZ appears to be about 250 μm in width at this location. The OIM results are in the form of IQ maps, discrete pole figures and misorientation angle distributions for scans that each have areas of 100 x 100 μm^2. The α grains just inside the SZ are very fine, equiaxed and ~ 5 μm in size in the IQ map in Fig. 8(b), and the α grains are interspersed with dark-etching features that are transformation products of the β which formed after dissolution of the eutectoid constituent. The boundary between the SZ and base metal is very sharp in the OM image of Fig. 4(a) although the α (sub)grain size in the IQ maps appears to be nearly constant throughout this region. The pole figure data from locations inside the SZ/TMAZ boundary indicates a random texture, as seen in Fig. 4(b), while a single lattice orientation becomes apparent upon crossing the boundary, as seen in Fig. 4(c). This orientation may be interpreted as a shear texture component, {111}<110>, at the intersection of the A-fiber, {111}<uvw>, and B-fiber, {hkl}<110>. The notation

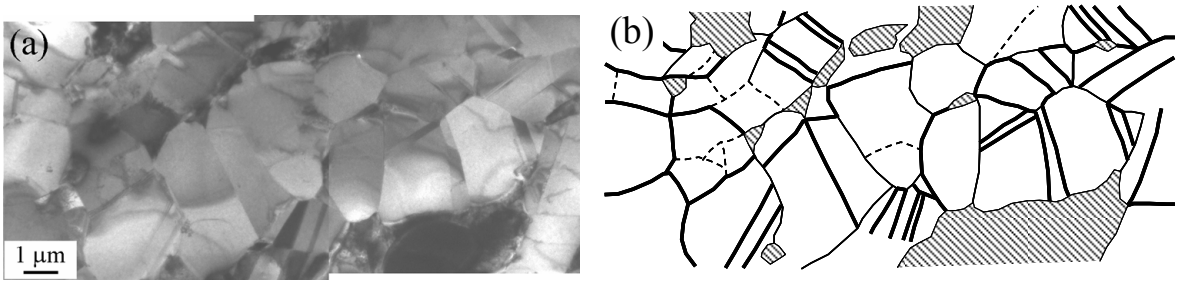

Fig. 3. Highly refined grains are apparent in the TEM images of (a); CBED analysis in (b) shows that the boundaries are mainly high-angle or twin boundaries.

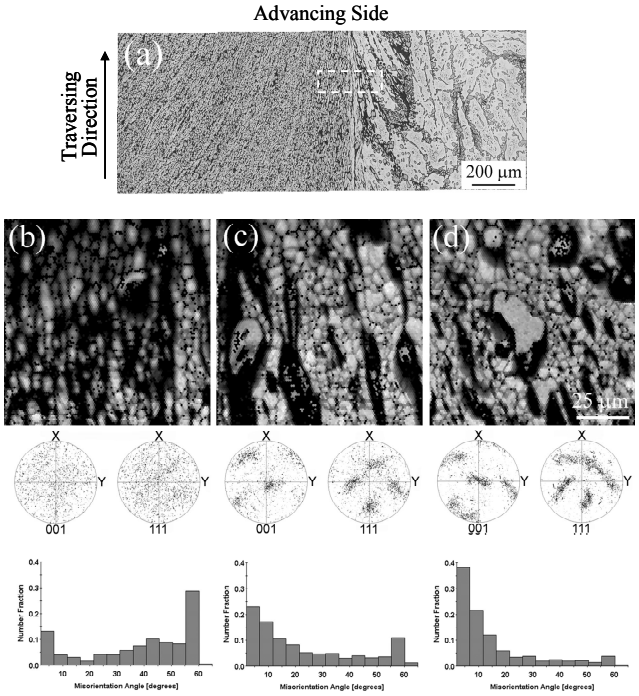

Fig. 4. OM and OIM data from location F on the advancing side of a SZ, illustrating the sharp transition from refined, recrystallized material in the the SZ to deformed and recovered material in the TMAZ.

refers to {the plane parallel to shear plane}<the direction parallel to shear direction> [26]; this interpretation requires the assumption that the strain state in the TMAZ is a simple shear on a plane approximately parallel to the local SZ/TMAZ interface and in a direction aligned with the traversing direction. In Fig. 4(d), at a location farther into the TMAZ, large lattice rotation from the orientation observed in Fig. 4(c) to another orientation has become apparent and the random component is less distinct. The second orientation does not correspond to a shear texture component aligned with the SZ/TMAZ interface.

Altogether, these data suggest that the SZ/TMAZ interface is a distinct boundary separating recrystallized and deformed and annealed material. The SZ microstructures and microstructure-based estimates of local SZ temperature indicate the temperature at the SZ/TMAZ interface is ~800 ºC and that severe deformation begins as the local temperature exceeds this value upon tool approach to a location along its path. At this temperature 1 - 10 μm κ_{iv} particles will persist in α grains. Severe deformation will generate localized deformation zones around these particles. For lattice-diffusion control of deformation and recovery, the strain rate necessary to achieve particle stimulated nucleation (PSN) of recrystallization is given by [27] $\dot{\varepsilon}_{PSN} \geq \frac{K_1}{d_p^2 T}\exp\left(-\frac{Q_D}{kT}\right)$, where $K_1 = \frac{\Omega G D_{0,l}}{k}$.

Here, Ω is the atom volume, G is the shear modulus, $D_{0,l}$ is the preexponential factor for lattice diffusion, k is Boltzmann's constant, d_P is the particle diameter, T is the temperature and $Q_{D,l}$ is the activation energy for lattice diffusion. When the local strain rate is sufficient to satisfy equation (1), local lattice rotations will lead to the formation of deformation zones around particles and support nucleation of new grains at the particles. Lattice-diffusion control may be assumed because of the high local temperatures, and, so, terms involving boundary diffusion have been omitted from equation (1). Using data for Cu [28] and taking d_p ~5 μm for the κ_{iv} particles and the temperature T = 800°C at the SZ/TMAZ interface, the strain rate for PSN is $\dot{\varepsilon}_{PSN} = 9\times10^{-3}$ s^{-1}. Modeling has indicated that $\dot{\varepsilon}_{local} \approx 200$ s^{-1} in the SZ near the pin surface during FSP of NAB materials [29]; the process is characterized by steep gradients in strain rate and temperature and so PSN is a plausible mechanism for recrystallization in the primary α at the SZ/TMAZ interface. Typically, PSN results in random lattice orientations of the recrystallized grains due to the random nature of the local lattice reorientations in the deformation zones around the particles and this would account for the random textures nearby the SZ/TMAZ interface in the lower SZ.

Acknowledgements The processed materials were provided by Mr. M.W. Mahoney, Rockwell Scientific Corporation, Thousand Oaks, CA and the Naval Surface Warfare Center - Carderock Div, Bethesda, MD. Funding for this work was provided by the Defense Advanced Research Projects Agency with Dr. Leo Christodoulou as program monitor.

Reference

[1] W.M. Thomas, E.D. Nicholas, J.C. Needham, M.G. Murch, P. Templesmith and C.J. Daws: G.B. Patent Application No. 9125978.8, December, 1991; U.S. Patent No. 5460317, October, 1995.
[2] R.S. Mishra: Adv. Mater. Proc. Vol. 161 (2003), p. 43
[3] R.S. Mishra, Z.Y. Ma and I. Charit: Mater. Sci. Engng. A Vol. A341 (2003) p. 307
[4] Z.Y. Ma, R.S. Mishra and M. W. Mahoney: *Friction Stir Welding and Processing II* (TMS, Warrendale, PA, 2003, eds. K.V. Jata, M.W. Mahoney, R.S. Mishra, S.L. Semiatin and T. Lienert) pp. 221-30
[5] R.S. Mishra, M.W. Mahoney, S.X. McFadden, N.A. Mara and A.K. Mukherjee: Scripta Mater. Vol. 42 (2000) p. 163
[6] R.S. Mishra and M.W. Mahoney: Mater. Sci. Forum Vol. 357-359 (2001) p. 507
[7] Z.Y. Ma, R.S. Mishra and M.W. Mahoney: Acta Mater. Vol. 50 (2002) p. 4419
[8] I. Charit and R.S. Mishra: Mater. Sci. Eng. A Vol. A359 (2003) p. 290
[9] Z.Y. Ma, R.S. Mishra M.W. Mahoney, R. Grimes: Mater. Sci. Eng. A Vol. A351 (2003) p. 148
[10] Y.S. Sato, M. Urata and H. Kokawa: Metal. Mater. Trans. A Vol. 33A (2002) p. 625
[11] S.H.C. Park, Y.S. Sato and H. Kokawa: Scripta Mater. Vol. 49 (2003) p.161
[12 D. Zhang, M. Suzuki and K. Maruyama: Scripta Mater. Vol. 52 (2005) p. 899
[13] H.S. Park, T. Kimura, T. Murakami, Y. Nagano, K. Nakata and M. Ushio: Mater. Sci. Eng. A, , Vol. A371 (2004) p. 160
[14] Y.S. Sato, T.W. Nelson and C.J. Sterling: Acta Mater. Vol. 53 (2005) p. 637
[15] A.P. Reynolds, E. Hood and W. Tang: Scripta Mater. Vol. 52 (2005) p. 491
[16] M.W. Mahoney, W.H. Bingel, S.R. Sharma and R.S. Mishra: Mater. Sci. Forum Vol. 426 (2003) p. 2843
[17] K. Oh-ishi, A. P. Zhilyaev, R. Williams and T. R. McNelley: *Friction Stir Welding and Processing III* (TMS, Warrendale, PA, 2005, eds. K.V. Jata, M.W. Mahoney, R.S. Mishra and T.J. Lienert) p. 107
[18] I. Charit and R.S. Mishra: Acta Mater. Vol. 53 (2005) p. 4211
[19] K. Oh-ishi and T.R. McNelley: Metall. Mater. Trans. A Vol. 35A (2004) p. 2951
[20] K. Oh-ishi and T.R. McNelley: Metall. Mater. Trans. A Vol. 36A (2005) p. 1575
[21] J.L. Robbins, O.C. Shepard and O.D. Sherby: J. Iron Steel Inst. Vol. 202 (1964) p. 804
[22] O.D. Sherby, B. Walser, C.M. Young and E.M. Cady: Scripta Metall. Vol. 9 (1975) p. 569
[23] B. Walser and O.D. Sherby: Metall. Trans. A, Vol. 10A (1979) p. 1461
[24] P.B. Prangnell and C.P. Heason: Acta Mater. Vol. 53 (2005) p. 3179
[25] J.K. MacKenzie: Biometrika Vol. 45 (1958) p. 229
[26] G.R. Canova, U.F. Kocks and J.J. Jonas: Acta Metall. Vol. 32 (1984) p. 211
[27] F.J. Humphreys: Acta Metall. Vol. 25 (1977) p. 1323
[28] J. Askill: *Tracer Diffusion Data for Metals, Alloys and Simple Oxides* (IFI Plenum, New York, NY, 1970) pp. 32-45
[29] A. Askari, S. Silling, B.London and M.W. Mahoney: *Friction Stir Welding and Processing*, (TMS, Warrendale, PA, 2001, eds. K.V. Jata, M.W. Mahoney, R.S. Mishra, S.L. Semiatin and D. P. Fields) pp. 43-50